IEEE Access
Multidisciplinary : Rapid Review : Open Access Journal

Received December 16, 2020, accepted January 4, 2021, date of publication January 8, 2021, date of current version January 15, 2021.

Digital Object Identifier 10.1109/ACCESS.2021.3050149

Constitutive Modeling of Cemented Tailings Backfill With Different Saturation States Based on Particle Swarm Optimization and Support Vector Machine

ZHUOQUN YU, YONGYAN WANG, AND HAO WANG
School of Mechanical and Electrical Engineering, Qingdao University of Science and Technology, Qingdao 266061, China
Corresponding author: Yongyan Wang (0019030005@mails.qust.edu.cn)

This work was supported in part by the National Natural Science Foundation Project of China under Grant 51674149, and in part by the Shandong Provincial Natural Science Foundation, China, under Grant ZR2019MEE082.

ABSTRACT Mine tailings disposal has been a serious environmental issue for decades. The wide application of cemented tailings backfill (CTB) technology could indirectly abate tailings pollution by recycling the tailings for backfilling. CTB constitutive modeling helps with design by improving the understanding of its compressive behavior. This study focused on CTB intelligent constitutive modeling considering the coupled effects of the cement content and saturation state. An artificial intelligence model was established and utilized based on particle swarm optimization (PSO) and the support vector machine (SVM). CTB samples with different cement contents and water saturation states were prepared, and unconfined compression tests were conducted to obtain the dataset. We verified the feasibility of using integrated PSO and SVM (P-S) in the CTB constitutive model using experimental data. We analyzed model errors. The results showed that the CTB stress strain curve was complex and nonlinear and could be significantly affected by the saturation states. PSO was feasible and efficient for tuning the SVM hyperparameters. The lowest minimum MSE value of 0.0108 was achieved in the eighth iteration. The PSO and SVM modeling was indicated to be accurate in the CTB constitutive model (a high R-square value of 0.9935 and a low mean squared error value of 0.001664 were achieved on the testing set). This model may accelerate the CTB structure design process.

INDEX TERMS Machine learning, materials testing, mechanical variables measurement.

I. INTRODUCTION

Mineral resource extraction and processing creates great quantities of mine tailings worldwide. Improper tailings disposal may cause serious accidents and environmental problems. In recent years, cemented tailings backfill (CTB) has become a reliable and environmentally responsible method of recycling mine tailings [1]–[3]. Typical CTB material is the mixture of mine tailings, cement, and water [4]. After being mixed in the backfill station, fresh CTB mixtures are delivered to mine stopes by means of reticulated pipelines. Hardened CTB can be used in structures for preventing caving, roof falls, and enhancing pillars recovery [5]. Compared with hydraulic fill or cemented rock-fill, CTB has lower binder cost, higher tailings consumption, and higher productivity [6], [7]. These advantages have resulted in wide CTB technology use in operating mines around the world [8], [9], which could indirectly abate tailings pollution.

Mining work requires safe and stable underground voids, and CTB mechanical properties must be seriously considered during its design and application. Thus, many scientific works have studied CTB mechanical properties [5], [10]–[13]. The uniaxial compressive strength is one of the most widely used CTB mechanical property parameters as uniaxial compressive strength tests are relatively accessible and cost-effective [14]. For instance, Fall *et al.* [14] investigated the relationship between the mix proportions (cement content, water-to-cement ratio, etc.) and the CTB mechanical and flow properties. Cao *et al.* [7] investigated the compressive strength and toughness of the fiber-reinforced CTB through a series of compressive strength tests, and reported that compressive strength and ductility were improved after the introduction of the fiber into CTB.

In comparison to compressive strength values obtained from physical experiments, constitutive modeling is more

The associate editor coordinating the review of this manuscript and approving it for publication was Victor Sanchez.

important for predicting and assessing CTB mechanical properties. Researchers have widely used conventional models with specific mathematical expressions to approximate experimentally observed behavior [8], [15], [16]. For instance, Tu *et al.* [8] proposed a CTB constitutive model with two functions according to three physical theories. Cui and Fall [17] developed an evolving elastic-plastic model considering the cement hydration level. In addition, CTB structures in the stopes may face a complex environment with multiple physical processes [18]. Thus a thermal, hydraulic, mechanical, and chemical (THMC) coupling model was developed by Wu *et al.* [16]. However, a more effective modeling approach to represent the complex and nonlinear constitutive relations of CTB is using artificial intelligence technology. In recent years, intelligent algorithms have been used to modeling the constitutive relations of multifarious materials. For example, Wu et al [19] conducted a comparative study on the performance of constitutive models for alloyed steel using genetic algorithm (GA) and artificial neural network (ANN). They reported that the model modified by ANN obtained the highest accuracy. However, the model based on ANN had a few defects such as poor generalization performance and overfitting. It also had practical limitations where there is a small amount of data [20]. Support vector machine (SVM) may be an effective solution for circumventing these limitations [21]. Therefore, there has been an increasing interest in using SVM to modeling the constitutive relations of geotechnical materials recently [21], [22]. Hyperparameters can determine the accuracy of the model based on SVM, and it can be very hard to find the optimal hyperparameters based on intuition or by trying all combinations. Particle swarm optimization (PSO) can be a powerful tool for searching the optimal hyperparameters for SVM. Several researchers have managed to integrate PSO and SVM to successfully solve engineering problems such as detecting the leak location of pipelines and forecasting remaining engine life [20], [23]. However, there has been only one published study on the constitutive modeling of CTB using machine learning algorithm [24]. It is evident that far too little attention has been paid to the intelligent constitutive modeling of CTB. Due to the fine particles and low cement content of CTB, the constitutive relation of CTB can be very complex and nonlinear, and it can be difficult to obtain a satisfactory formulation to describe its constitutive relation concisely. Besides, CTB may have different water saturation states due to the effect of groundwater [25]–[27]. The saturation states may significantly affect the compressive behavior of CTB. However, there have been few studies on the feasibility of modeling the CTB constitutive relation considering water saturation states using artificial intelligence technology. It is not known whether machine learning algorithms can work well on the constitutive modeling of CTB with different saturation states.

In this paper, an artificial intelligence modeling method based on machine learning algorithms was used to learn the constitutive relations of CTB with different cement contents and water saturation states. Specifically, the support vector machine (SVM) was utilized to learn the stress strain relations and particle swarm optimization (PSO) was utilized for the hyperparameters tuning of the SVM to optimize its capability. Compared with the mathematical expressions, the proposed integrated PSO and SVM (P-S) modeling approach was expected to have much higher efficiency in the constitutive modeling of CTB.

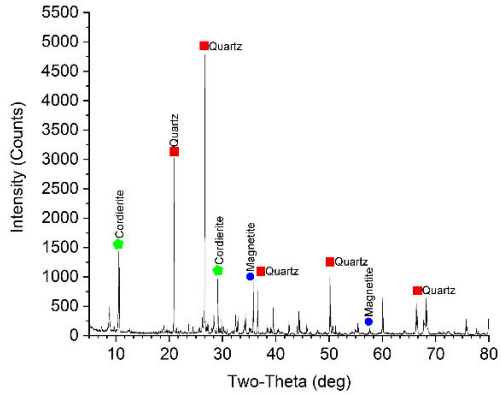

FIGURE 1. XRD pattern of the tailings.

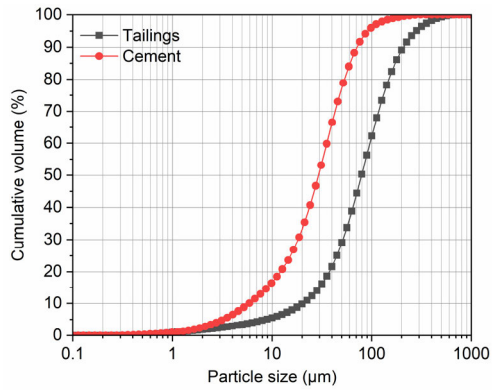

FIGURE 2. Particle size distribution of the tailings and cement.

II. MATERIALS AND METHODS

A. MATERIALS

The tailings used were sourced from an iron mine located in the southern part of Shandong, China. The mineralogical composition of the tailings identified by X-ray diffraction (XRD) is shown in Figure 1. A laser particle size analyzer (Mastersizer 3000, Malvern) was used to observe the particle size distribution. Ordinary Portland cement P.O. 42.5 provided by the Yangchun Cement Co. LTD in the Shandong Province, China was utilized as the binder. The particle size distribution curves of the cement and the tailings are presented in Figure 2. The most commonly employed cement contents in CTB are between 3% and 10%, according to the published literature [10], [11], [28], [29]. Therefore, cement contents utilized in this study were 5%, 7%, and 10% by dry weight of the tailings. The main chemical and physical properties of the tailings and cement are shown in Table 1. The mixing water employed to mix the cement

TABLE 1. Main chemical and physical properties of the tailings and cement.

Physical properties	tailings	cement	Chemical composition	tailings	cement
Specific gravity	2.76	3.10	SiO2	55.50	21.40
Specific surface (cm2/g)	2640	3580	Al2O3	2.93	4.31
D10 (μm)	20.41	6.66	Fe2O3	23.80	4.91
D50 (μm)	79.62	33.2	MgO	3.18	3.00
D90 (μm)	208.89	81.2	CaO	5.26	62.34
			SO3	0.41	2.20
			Na2O	0.62	—
			K2O	0.80	—
			P2O5	0.38	—
			MnO	0.21	—
			TiO2	0.12	—

TABLE 2. Details of the samples.

Group name and its state	A			B			C			D		
	Dried			Low saturated			Ideal cured			Fully saturated		
Sample designation	A5	A7	A10	B5	B7	B10	C5	C7	C10	D5	D7	D10
Target water content (%)	0	0	0	13	13	13	25	25	25	30	30	30
Cement content (%)	5	7	10	5	7	10	5	7	10	5	7	10

and tailings was tap water that met the Chinese National Standards GB5749 [30].

B. PREPARATION OF CTB SAMPLES

All materials used for the preparation of CTB samples were weighed on an electric scale with an accuracy of 0.01g. The solid content of the CTB mixtures was determined to be 75% constantly based on the practice experience of the source mine site. Dry tailings and cement were initially mixed in a laboratory mixer while the preweighed amount of water was slowly added to achieve the solid content of 75%. After seven minutes of mixing, the slurry was cast into a plastic cylindrical mold and cured for 12 hours at room temperature with a cap on it. After 12 hours, the 50 x 100 mm (diameter and height) sample was demolded and- placed in the curing chamber to be cured for 28 days. The curing relative humidity and temperature were kept at 95% and 20°, respectively. The CTB slurry slump range was measured to be 200 mm to 210 mm, which indicated a high workability for backfill operations.

After being cured for 28 days, CTB samples were divided into four groups (named A, B, C, and D). These groups underwent different treatments based on trial test results and ASTM C642 guidelines [31] to obtain the samples with different saturation states. The water content described in (1) was used to describe the saturation states [32]–[34].

$$\omega_c = \frac{m_c - m_d}{m_d} \times 100\% \tag{1}$$

where ω_c is the sample current water content (%); m_c is the sample current weight (g); m_d is the sample dry weight (g). The calculations were accurate to 1%. For group A, the samples were dried at 105° in a programmable temperature and humidity test chamber (Reale, RPH-80) for more than 24 hours until the sample weight remained constant. Then the weight of the dried sample was determined as the dry weight of the sample, and the water content of the sample was determined to be 0%. The samples in group B were dried at 105° in the temperature and humidity test chamber for more than 6 hours. Then the sample was weighed at set intervals, and the current water content was calculated immediately. Once the current water content reached the target value, the drying process was terminated. For group C, the CTB samples were weighed and ready for testing without treatment as the ideal cured CTB. The samples in group D were soaked in boiling water for more than 6 hours until the sample weight remained constant to represent fully saturated CTB. Table 2 lists the sample details including group name, sample designation, saturation states, target water contents, and cement contents.

C. UNCONFINED COMPRESSION TEST

A series of unconfined compression tests were operated to obtain the stress strain relations of CTB samples under different conditions. The unconfined compression test methods for CTB was determined based on previous studies [10], [35] and ASTM C39 [36] guidelines. A computer-controlled mechanical press system was used in carrying out the tests. Test samples were placed axially between the two bearing plates and loaded at a constant displacement rate of 0.2 mm/min.

III. ALGORITHMS AND MODELING METHODS

A. SUPPORT VECTOR MACHINE

SVM is a well-established supervised learning method first developed firstly by Vapnik [37], Cortes and Vapnik [38]. In recent years, SVM has been utilized in various scientific fields for prediction, classification, and regression analysis [22], [39]–[42]. SVM was selected for the constitutive modeling in this study owing to its advantages such as effectiveness in high dimensional spaces, no required

assumption about the data distribution, and efficient principles that avoid overfitting [22], [43].

SVM maps data to the high dimensional space characteristic and establishes the following regression functions:

$$f(x) = w \cdot \phi(x) + b \tag{2}$$

$$R_{SVMs}(C) = \frac{1}{2}||w||^2 + C\frac{1}{n}\sum_{i=1}^{n} L(x_i, d_i) \tag{3}$$

where the unknown parameters w and b are the weight vector and the hyperplane bias term, respectively; $\phi(x)$ is the nonlinear mapping that mapped the vector x from low-dimensional space to high-dimensional space; C indicates the penalty coefficient, and $L(x_i, d_i)$ stands for the Lagrange multiplier. The optimum parameters w and b can be determined by minimizing the objective function as presented in (4), with the constraints shown in (5):

$$R_{SVMs}\left(w, \xi^{(*)}\right) = \frac{1}{2}||w||^2 + C\sum_{i=1}^{n}\left(\xi_i + \xi_i^*\right) \tag{4}$$

$$s.t \begin{cases} d_i - w \cdot \phi(x_i) + b \le \varepsilon + \xi_i, & i = 1, \ldots, n \\ w \cdot \phi(x_i) + b - d_i + \xi_i^*, & i = 1, \ldots, n \\ \xi_i, \xi_i^* \ge 0, & i = 1, \ldots, n \end{cases} \tag{5}$$

where ξ_i and ξ_i^* indicate the positive slack variables; ε is the (in)sensitivity (i.e. the maximum misclassification error allowed). A generic function as represented in (6) is proposed to solve the optimal regression function:

$$y = \sum_{i=1}^{n}\left(a_i - a_i^*\right)K(x, x_i) + b \tag{6}$$

where a_i and a_i^* are the Lagrange multipliers;$K(x, x_i)$ is the kernel function. And the radial basis kernel function (RBF) was chosen in this study owing to its transparency, high-efficiency, and adaptability [44]. The nonlinear RBF kernel is described as (7):

$$K(x, x_i) = e^{\left(-\gamma\|x - x_i\|^2\right)} \tag{7}$$

where x and x_i are input space vectors; γ is defined as $\gamma = \frac{1}{2\sigma^2}$; and σ^2 is the squared variance of the Gaussian function.

B. PARTICLE SWARM OPTIMIZATION

PSO was first built up by Kennedy and Eberhart [45]. It was a nature inspired optimization algorithm which has been used for optimizing various engineering problems [46]–[50]. In this study, the parameters of SVM were tuned using PSO.

PSO process starts with a randomly generated swarm of particles with each particle representing a dot in the n-dimensional space. Each particle has its own velocity and location which are continuously affected by the latest information of personal best (pbest) and global best (gbest) in the particle swarm based on the following functions:

$$v_i^{k+1} = w_i v_i^k + c_1 r_1\left(p_{best,i}^k - x_i^k\right) + c_2 r_2\left(g_{best,i}^k - x_i^k\right) \tag{8}$$

$$x_i^{k+1} = x_i^k + v_i^{k+1} \tag{9}$$

TABLE 3. SVM hypeparameters and their tuning ranges.

Hyperparameters	Explanation	Range
C	penalization parameter	0.01-10
ε	insensitivity	0.0001-0.1
γ	Parameter of the kernel function	0.01-1000

where k determines the iteration number; i is the particle sequence number; w, c_1, and c_2 are global parameters named inertia weight; r_1 and r_2 are random values dotted between the range of [0, 1].

C. ESTABLISHMENT AND VERIFICATION OF THE P-S MODEL

The SVM and PSO algorithms were integrated as the P-S model for the constitutive modeling of CTB. The P-S model used PSO to tune hyperparameters and optimize the SVM model, since parameters C, ε and γ had significant influence on the performance of the SVM model. The experimental data obtained from the unconfined compression tests were utilized to build the dataset. This dataset will serve as a data source for the establishment and verification of the P-S model. The hyperparameters of SVM were tuned by PSO on the training set. The k-fold cross-validation (CV) was carried out to find the optimal hyperparameters for the SVM model. According to the trial tests and recommendations in the literature [23], [40], [50], k was determined to be 5; the PSO parameters w, c_1, and c_2 were set to be $\frac{1}{2\ln 2}$, $0.5 + \ln 2$, and $0.5 + \ln 2$, respectively; the swarm size and the maximum iteration were determined to be 20 and 50, respectively; the tuned hyper-parameters of SVM and their corresponding ranges are shown in Table 3. After the optimal hyperparameters were obtained, the P-S model was established using these parameters. The whole training set was used to train the optimal P-S model, and the trained P-S model was verified on the testing set with R-square (R^2) and mean squared error (MSE) values. Figure 3 is the flowchart of the P-S model.

IV. RESULTS AND DISCUSSION

A. STRESS STRAIN RELATIONS

The stress strain diagrams (Figure 4) were produced according to the loading data of the CTB samples in the unconfined compression tests. It can be seen from Figure 4 that most CTB stress strain curves shared many common features. For example, the stress strain curves of CTB samples generally included several stages and nonlinear curves. At the very beginning of the stress strain curves, the stress increased slowly with increasing strain. In this stage, the bearing plate was adjusting to the surface of the sample, and the pores of the sample were closing. After that, the stress increased sharply and the course of the stress strain curve was almost linear. At that stage, there was elastic deformation. When the plastic deformation started, the increase of the stress slowed down and the course of the stress strain curve was nonlinear. During this stage, the sample was undergoing plastic deformation and

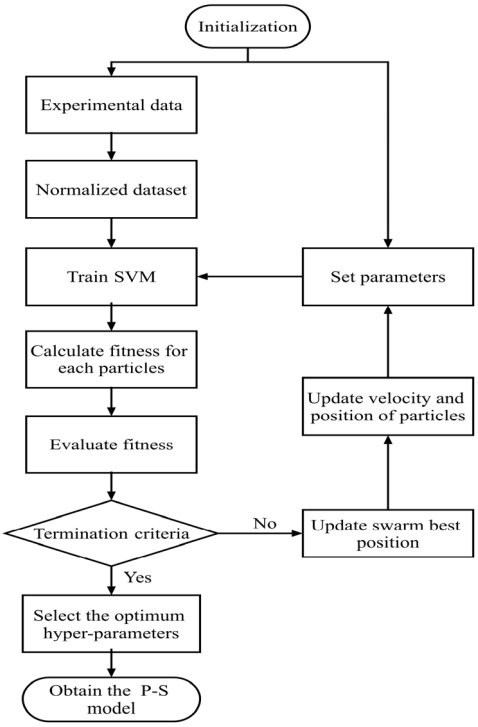

FIGURE 3. Flowchart of the establishment of P-S model.

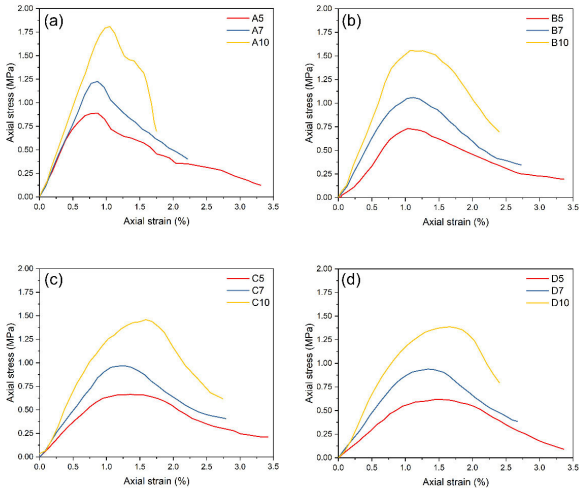

FIGURE 4. CTB samples stress strain diagrams: (a) group A, water content = 0%; (b) group B, water content = 13%, (c) group C, water content = 25%; and (d) group D, water content = 30%.

began to destruct until the sample reached its peak strength (i.e. the unconfined compressive strength). After attaining the peak strength, the stress was decreased gradually with increasing strain, which was named the postpeak fracture stage.

However, it can also be seen from Figure 4 that the detailed characteristic of the stress strain relation varied greatly with the coupled influence of cement and water contents. The unconfined compressive strength of the CTB sample increased with the increase of cement content. This may have been due to increased cement content giving rise

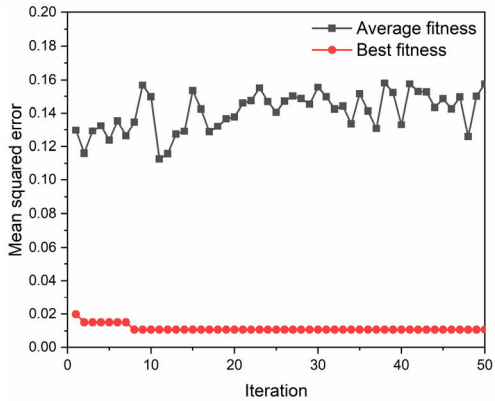

FIGURE 5. Fitness curves of hyperparameters tuning using PSO.

to an increasing amount of hydration products and therefore strengthening the hardened CTB [51]. It can also be seen that the unconfined compressive strength decreased with the increase of the water content, and the stress strain curve dropped suddenly after failure when the water content was low. These results indicated that the cement content and water content can significantly affected the stress strain relations of CTB. There are two reasons for this result: (i) more hydration products produced by cement have led to significant increase in the stiffness and brittleness of CTB [52]–[54]; and (ii) water could have reduced the friction between the particles in CTB and accelerated the propagation of micro-cracks, thus reducing compressive strength [33], [55].

For the constitutive modeling of CTB, the data set was built based on the experimental stress strain values. According to the experience of the intelligent constitutive modeling of CTB [24], experimental data with a strain interval of 0.10% were selected. The input variables for the P-S were the cement content, the water content, and the strain. The output variable was the stress. The dataset contained 380 samples with three features. The dataset was split into two subsets, the training set and the test set, with a size ratio of 7:3. In order to accelerate the computational efficiency and improve the accuracy, the input data were scaled to the $[-1, 1]$ range.

B. RESULTS OF HYPERPARAMETERS TUNING

During the hyperparameters tuning process using PSO, the fitness values were being recorded to draw the fitness curves. The average fitness (i.e., the average MSE) and the best fitness (i.e., the minimum MSE) curves are shown in Figure 5. It can be seen that the average fitness values ranged from 0.1127 to 0.1575 in the first 50 iterations. The minimum MSE value decreased from 0.01981 to 0.1514 in the second iteration. After that, the minimum MSE decreased from 0.1575 to 0.0108at the eighth iteration and then kept constant. The lowest minimum MSE of 0.0108 was achieved only after eight iterations. These results indicated that the PSO was efficient and feasible in tuning the hyperparameters for SVM. The detailed information about the obtained optimal hyperparameters is listed in Table 4. The P-S model was built based on the obtained optimal hyperparameters for the

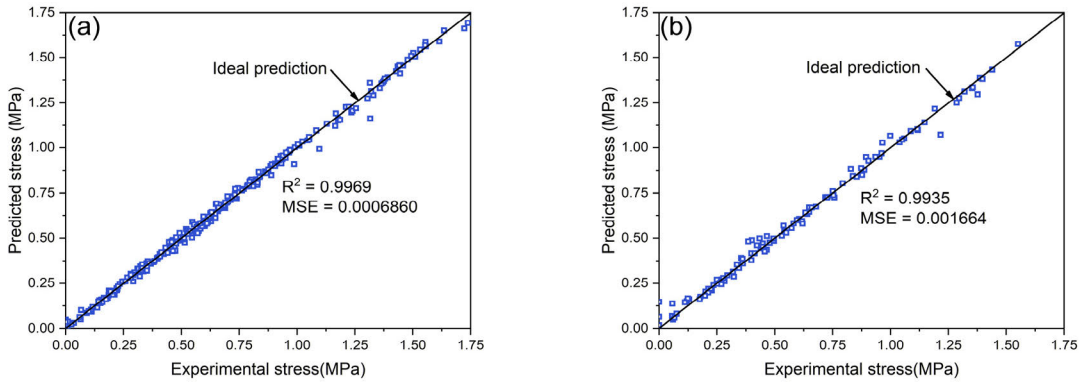

FIGURE 6. Capability of the P-S model on (a) the training set and (b) the testing set.

TABLE 4. Optimal SVM hyperparameters.

Hyperparameters	Explanation	Range
C	penalization parameter	4.6533
ε	insensitivity	0.0968
γ	Parameter of the kernel function	8.7061

constitutive modeling of CPB samples at different saturation states.

C. CAPABILITY OF THE P-S MODEL

The capability of the established P-S model on the training set and testing set is presented in Figure 6. It can be observed that the established model exhibited a high capability for modeling of constitutive relations of CTB. According to the verification results, high R^2 values of 0.9969 and 0.9935 were achieved on the training set and testing set, respectively. Furthermore, low MSE values of 0.0006860 and 0.001664 were achieved, which demonstrated the established model's high accuracy. The R^2 values of 0.9935 on the testing set was very close to the R^2 values of 0.9969 on the training set, which indicated that the P-S model was well trained.

The stress values predicted by the trained P-S model along with the experimental stress strain diagrams obtained from the unconfined compression tests are presented in Figure 7 for comparison. It can be observed that the stress values predicted by the P-S model were generally consistent with the experimental stress values, which indicated that the optimal P-S model was successful in modeling the constitutive relation of CTB with different cement contents and saturation states (represented by different water contents). Compared to the previous study on the constitutive modeling of cemented paste backfill based on the random forest (RF) and firefly algorithm (FA), which also had a well performance (R value = 0.989 on the testing set) [24]. The P-S model in this study seems to have been more suitable for smaller data amounts, which was determined by the nature of the algorithms. RF cannot extrapolate when the predicted values are outside the training set values. This may have been responsible for the abnormal outliers in the previous study [24]. In this study, the SVM successfully avoided the defects of RF and there were no abnormal outliers in the predicted results. There were only several large errors near the peak, the end, and the strain-softening stages of the stress strain curve. Fortunately, these large errors were explicable and acceptable in the constitutive modeling of CTB according to the experimental analysis and the published literature [8], [15]. As discussed above, the sudden failure of the dried sample may have caused a rapid drop in the stress. On the other hand, the peak of the stress strain curves was the demarcation point of two completely different stages of the stress strain curve namely the pre-peak elastoplastic stage and the post-peak fracture stage. Therefore, the stress strain curve showed a sharp turn near its peak where the stress changed dramatically with the strain. This may have been responsible for the large errors in the stress strain curves of dried samples. In addition, large errors near the stress strain curve ends as shown in Figure 7(b) may have been due to the lack of training data at the end of the stress strain curves [24]. During the unconfined compression test, it was observed that there were usually clear cracks in the sample and even collapsed with falling blocks, especially for the dried sample. A digital camera was used to record images of the sample during the unconfined compression test. Pictures of a typical dried sample at the prepeak and postpeak stage are shown in Figure 8. It can be seen from Figure 8(a) that there was no crack visible to the naked eye at the prepeak stage. However, a major crack could be clearly distinguished at the postpeak stage, and there was a deletion on the top section of the sample as shown in Figure 8(b). The rapid development of major cracks and unexpected fall of blocks may have caused the sudden fluctuation at the strain-softening stage of the stress strain curves, which may be have been responsible for the large errors observed at the strain-softening stage of the stress strain curves as shown in Figures 7(a) and (c).

Besides, the proposed modeling method based on SVM and PSO has high computational efficiency. The average computational time is 20 seconds, using MATLAB 2017a on a personal computer with Intel Core i5-6300u 2.5 GHz processor and 8 GB RAM.

As a result, the P-S model established in this study was feasible and efficient for the constitutive modeling of CTB

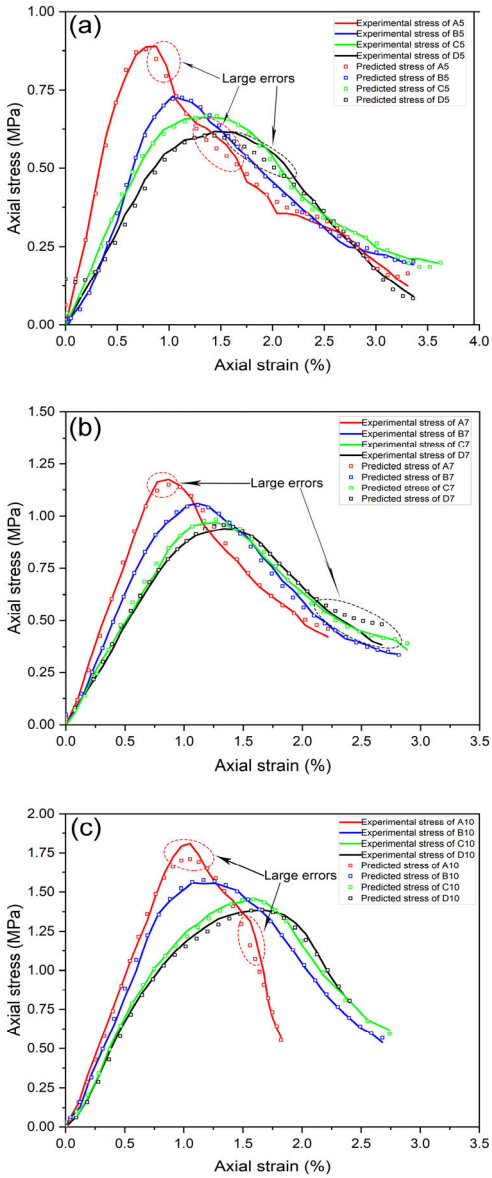

FIGURE 7. Comparison of the predicted and experimental stress strain diagrams: (a) cement content = 5%; (b) cement content = 7%; (c) cement content = 10%.

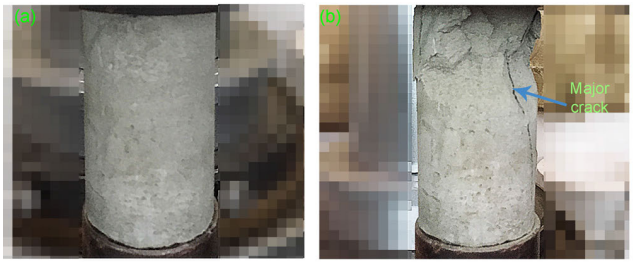

FIGURE 8. Pictorial view of the dried sample at the (a) pre-peak elastoplastic stage and (b) post-peak fracture stage.

with different saturation states. This modeling approach extends the recent efforts for intelligent constitutive modeling of CTB. This approach is expected to provide an efficient way to obtain an accurate constitutive model to help to understand the compressive behavior of CTB, and to accelerate the CTB structure design process.

V. CONCLUSION

In this study, CTB samples with different cement contents and saturation states were prepared. Unconfined compression tests were carried out for these samples. The P-S model was established for the constitutive modeling of CTB. The capability of the optimal model was verified by R^2 and MSE. Furthermore, large errors were analyzed and discussed. On the basis of the achieved findings, the following conclusions could be drawn:

•The stress strain curve of CTB was generally composed of several different stages, which was complex and non-linear. The cement content and saturation state had significant effects on the constitutive relation of CTB.

•PSO was efficient and feasible for tuning SVM hyperparameters. The minimum MSE value decreased significantly in the second iteration, and the optimal hyperparameters were achieved with the lowest minimum MSE value of 0.0108 in the eighth iteration.

•The optimal hyperparameters of SVM model utilized in this study were $C = 4.6533$, $\varepsilon = 0.0968$ and $\gamma = 8.7061$. A high R^2 value of 0.9935 and a low MSE value of 0.001664 were achieved on the testing set, indicating that the P-S model was feasible in the constitutive modeling of CTB with different saturation states. On the whole, the P-S model had decent accuracy. The errors mainly came from the results in group A, which have been explained well.

•The P-S model successfully avoided defects from the RF model in the previous study. No abnormal outliers were found in the predicted results. There were only several large errors concentrated near the peak, the end, and the strain-softening stage of the stress strain curve. The sudden failure of the CTB sample and the lack of training data at the end of the stress strain curves may have been responsible for the appearance of these errors.

These findings indicated that the approach based on the P-S model was efficient and accurate for the constitutive modeling of CTB. It is expected to help in understanding the compressive behavior of CTB and accelerate the CTB structure design process.

ACKNOWLEDGMENT

The authors would like to acknowledge the materials supply and technical supports from Shandong Gold Mining Company, Ltd.

REFERENCES

[1] F. Beya, M. Mbonimpa, T. Belem, L. Li, U. Marceau, P. Kalonji, M. Benzaazoua, and S. Ouellet, "Mine backfilling in the permafrost, part I: Numerical prediction of thermal curing conditions within the cemented paste backfill matrix," *Minerals*, vol. 9, no. 3, p. 165, Mar. 2019.

[2] A. Ghirian and M. Fall, "Coupled thermo-hydro-mechanical–chemical behaviour of cemented paste backfill in column experiments," *Eng. Geol.*, vol. 170, pp. 11–23, Feb. 2014.

[3] Q. Chen, Q. Zhang, A. Fourie, and C. Xin, "Utilization of phosphogypsum and phosphate tailings for cemented paste backfill," *J. Environ. Manage.*, vol. 201, pp. 19–27, Oct. 2017.

[4] J. Li, E. Yilmaz, and S. Cao, "Influence of solid content, cement/tailings ratio, and curing time on rheology and strength of cemented tailings backfill," *Minerals*, vol. 10, no. 10, p. 922, Oct. 2020.

[5] S. Huang, K. Xia, and L. Qiao, "Dynamic tests of cemented paste backfill: Effects of strain rate, curing time, and cement content on compressive strength," *J. Mater. Sci.*, vol. 46, no. 15, pp. 5165–5170, Aug. 2011.

[6] O. Nasir and M. Fall, "Coupling binder hydration, temperature and compressive strength development of underground cemented paste backfill at early ages," *Tunnelling Underground Space Technol.*, vol. 25, no. 1, pp. 9–20, Jan. 2010.

[7] S. Cao, E. Yilmaz, and W. Song, "Fiber type effect on strength, toughness and microstructure of early age cemented tailings backfill," *Construct. Building Mater.*, vol. 223, pp. 44–54, Oct. 2019.

[8] B. Tu, L. Liu, K. Cheng, B. Zhang, Y. Zhao, Q. Yang, and K. Song, "A constitutive model for cemented tailings backfill under uniaxial compression," *Frontiers Phys.*, vol. 8, p. 173, Jul. 2020.

[9] G. Xue, E. Yilmaz, W. Song, and S. Cao, "Fiber length effect on strength properties of polypropylene fiber reinforced cemented tailings backfill specimens with different sizes," *Construct. Building Mater.*, vol. 241, Apr. 2020, Art. no. 118113.

[10] X. W. Yi, G. W. Ma, and A. Fourie, "Compressive behaviour of fibre-reinforced cemented paste backfill," *Geotextiles Geomembranes*, vol. 43, no. 3, pp. 207–215, Jun. 2015.

[11] M. Fall, T. Belem, S. Samb, and M. Benzaazoua, "Experimental characterization of the stress–strain behaviour of cemented paste backfill in compression," *J. Mater. Sci.*, vol. 42, no. 11, pp. 3914–3922, Jun. 2007.

[12] Q.-S. Chen, Q.-L. Zhang, A. Fourie, X. Chen, and C.-C. Qi, "Experimental investigation on the strength characteristics of cement paste backfill in a similar stope model and its mechanism," *Construct. Building Mater.*, vol. 154, pp. 34–43, Nov. 2017.

[13] E. Yilmaz, T. Belem, B. Bussière, M. Mbonimpa, and M. Benzaazoua, "Curing time effect on consolidation behaviour of cemented paste backfill containing different cement types and contents," *Construct. Building Mater.*, vol. 75, pp. 99–111, Jan. 2015.

[14] M. Fall, M. Benzaazoua, and E. G. Saa, "Mix proportioning of underground cemented tailings backfill," *Tunnelling Underground Space Technol.*, vol. 23, no. 1, pp. 80–90, Jan. 2008.

[15] L. Cui and M. Fall, "Multiphysics modeling and simulation of strength development and distribution in cemented tailings backfill structures," *Int. J. Concrete Struct. Mater.*, vol. 12, no. 1, p. 25, Dec. 2018.

[16] D. Wu, T. Deng, and R. Zhao, "A coupled THMC modeling application of cemented coal gangue-fly ash backfill," *Construct. Building Mater.*, vol. 158, pp. 326–336, Jan. 2018.

[17] L. Cui and M. Fall, "An evolutive elasto-plastic model for cemented paste backfill," *Comput. Geotechnics*, vol. 71, pp. 19–29, Jan. 2016.

[18] L. Cui and M. Fall, "Multiphysics modeling of arching effects in fill mass," *Comput. Geotechnics*, vol. 83, pp. 114–131, Mar. 2017.

[19] S.-W. Wu, X.-G. Zhou, G.-M. Cao, Z.-Y. Liu, and G.-D. Wang, "The improvement on constitutive modeling of Nb-Ti micro alloyed steel by using intelligent algorithms," *Mater. Des.*, vol. 116, pp. 676–685, Feb. 2017.

[20] L. Ni, J. Jiang, and Y. Pan, "Leak location of pipelines based on transient model and PSO-SVM," *J. Loss Prevention Process Industries*, vol. 26, no. 6, pp. 1085–1093, Nov. 2013.

[21] H. Zhao, Z. Huang, and Z. Zou, "Simulating the stress-strain relationship of geomaterials by support vector machine," *Math. Problems Eng.*, vol. 2014, pp. 1–7, Jan. 2014.

[22] X. Zhou and J. Shen, "Least squares support vector machine for constitutive modeling of clay," *Int. J. Eng.*, vol. 28, no. 11, pp. 1571–1578, 2015.

[23] P. J. G. Nieto, E. García-Gonzalo, F. S. Lasheras, and F. J. de Cos Juez, "Hybrid PSO–SVM-based method for forecasting of the remaining useful life for aircraft engines and evaluation of its reliability," *Rel. Eng. Syst. Saf.*, vol. 138, pp. 219–231, Jun. 2015.

[24] C. Qi, Q. Chen, A. Fourie, X. Tang, Q. Zhang, X. Dong, and Y. Feng, "Constitutive modelling of cemented paste backfill: A data-mining approach," *Construct. Building Mater.*, vol. 197, pp. 262–270, Feb. 2019.

[25] R. Hamberg, C. Maurice, and L. Alakangas, "Lowering the water saturation level in cemented paste backfill mixtures—Effect on the release of arsenic," *Minerals Eng.*, vol. 112, pp. 84–91, Oct. 2017.

[26] R. Hamberg, C. Maurice, and L. Alakangas, "The formation of unsaturated zones within cemented paste backfill mixtures—Effects on the release of copper, nickel, and zinc," *Environ. Sci. Pollut. Res.*, vol. 25, no. 21, pp. 20809–20822, Jul. 2018.

[27] S. Ouellet, B. Bussière, M. Mbonimpa, M. Benzaazoua, and M. Aubertin, "Reactivity and mineralogical evolution of an underground mine sulphidic cemented paste backfill," *Minerals Eng.*, vol. 19, no. 5, pp. 407–419, Apr. 2006.

[28] H. Jiang, Z. Qi, E. Yilmaz, J. Han, J. Qiu, and C. Dong, "Effectiveness of alkali-activated slag as alternative binder on workability and early age compressive strength of cemented paste backfills," *Construct. Building Mater.*, vol. 218, pp. 689–700, Sep. 2019.

[29] M. B. C. Mangane, R. Argane, R. Trauchessec, A. Lecomte, and M. Benzaazoua, "Influence of superplasticizers on mechanical properties and workability of cemented paste backfill," *Minerals Eng.*, vol. 116, pp. 3–14, Jan. 2018.

[30] *Standards for Drinking Water Quality*, Standard GB5749, 2006.

[31] *Standard Test Method for Density, Absorption, and Voids in Hardened Concrete*, Standard ASTM C642, 2013.

[32] E. I. Stavridakis, "Evaluation of engineering and cement–stabilization parameters of Clayey–Sand mixtures under soaked conditions," *Geotech. Geol. Eng.*, vol. 23, no. 6, pp. 635–655, Nov. 2005.

[33] L. S. Ho, K. Nakarai, Y. Ogawa, T. Sasaki, and M. Morioka, "Strength development of cement-treated soils: Effects of water content, carbonation, and pozzolanic reaction under drying curing condition," *Construct. Building Mater.*, vol. 134, pp. 703–712, Mar. 2017.

[34] *Specifications for Rock Tests in Water Conservancy and Hydropower Engineering*, Standard SL 264-2001, 2001.

[35] X. Chen, X. Shi, J. Zhou, Q. Chen, E. Li, and X. Du, "Compressive behavior and microstructural properties of tailings polypropylene fibre-reinforced cemented paste backfill," *Construct. Building Mater.*, vol. 190, pp. 211–221, Nov. 2018.

[36] *Standard Test Method for Compressive Strength of Cylindrical Concrete Specimens*, Standard ASTM C39, 2002.

[37] V. N. Vapnik, "An overview of statistical learning theory," *IEEE Trans. Neural Netw.*, vol. 10, no. 5, pp. 99–988, Sep. 1999.

[38] C. Cortes and V. Vapnik, "Support-vector networks," *Mach. Learn.*, vol. 20, no. 3, pp. 273–297, 1995.

[39] L. Olatomiwa, S. Mekhilef, S. Shamshirband, K. Mohammadi, D. Petković, and C. Sudheer, "A support vector machine–firefly algorithm-based model for global solar radiation prediction," *Sol. Energy*, vol. 115, pp. 632–644, May 2015.

[40] V. Rodriguez-Galiano, M. Sanchez-Castillo, M. Chica-Olmo, and M. Chica-Rivas, "Machine learning predictive models for mineral prospectivity: An evaluation of neural networks, random forest, regression trees and support vector machines," *Ore Geol. Rev.*, vol. 71, pp. 804–818, Dec. 2015.

[41] S. Shamshirband, K. Mohammadi, H. Khorasanizadeh, P. L. Yee, M. Lee, D. Petković, and E. Zalnezhad, "Estimating the diffuse solar radiation using a coupled support vector machine–wavelet transform model," *Renew. Sustain. Energy Rev.*, vol. 56, pp. 428–435, Apr. 2016.

[42] J. Zhang, X. Lin, and X. Ning, "SVM-based classification of segmented airborne LiDAR point clouds in urban areas," *Remote Sens.*, vol. 5, no. 8, pp. 3749–3775, Jul. 2013.

[43] E. M. Abdel-Rahman, O. Mutanga, E. Adam, and R. Ismail, "Detecting sirex noctilio grey-attacked and lightning-struck pine trees using airborne hyperspectral data, random forest and support vector machines classifiers," *ISPRS J. Photogramm. Remote Sens.*, vol. 88, pp. 48–59, Feb. 2014.

[44] K.-P. Wu and S.-D. Wang, "Choosing the kernel parameters for support vector machines by the inter-cluster distance in the feature space," *Pattern Recognit.*, vol. 42, no. 5, pp. 710–717, May 2009.

[45] J. Kennedy and R. Eberhart, "Particle swarm optimization," presented at the Int. Conf. Neural Netw. (ICNN), 1995.

[46] H. Melo and J. Watada, "Gaussian-PSO with fuzzy reasoning based on structural learning for training a neural network," *Neurocomputing*, vol. 172, pp. 405–412, Jan. 2016.

[47] Z. Chen and L. Yu, "A new structural damage detection strategy of hybrid PSO with Monte Carlo simulations and experimental verifications," *Measurement*, vol. 122, pp. 658–669, Jul. 2018.

[48] S. Surya and R. Ravi, "MPSO-SHM: Modified PSO based structural health monitoring system for detecting the faulty sensors in WSN," *Wireless Pers. Commun.*, vol. 108, no. 1, pp. 141–157, Sep. 2019.

[49] N. Di Cesare and M. Domaszewski, "A new hybrid topology optimization method based on I-PR-PSO and ESO. Application to continuum structural mechanics," *Comput. Struct.*, vol. 212, pp. 311–326, Feb. 2019.

[50] C. Qi, A. Fourie, and Q. Chen, "Neural network and particle swarm optimization for predicting the unconfined compressive strength of cemented paste backfill," *Construct. Building Mater.*, vol. 159, pp. 473–478, Jan. 2018.
[51] L. Cui and M. Fall, "Mechanical and thermal properties of cemented tailings materials at early ages: Influence of initial temperature, curing stress and drainage conditions," *Construct. Building Mater.*, vol. 125, pp. 553–563, Oct. 2016.
[52] M. H. A. Beygi, M. T. Kazemi, I. M. Nikbin, and J. V. Amiri, "The effect of water to cement ratio on fracture parameters and brittleness of self-compacting concrete," *Mater. Des.*, vol. 50, pp. 267–276, Sep. 2013.
[53] J. S. Yadav and S. K. Tiwari, "Behaviour of cement stabilized treated coir fibre-reinforced clay-pond ash mixtures," *J. Building Eng.*, vol. 8, pp. 131–140, Dec. 2016.
[54] F. Schnaid, P. D. M. Prietto, and N. C. Consoli, "Characterization of cemented sand in triaxial compression," *J. Geotechnical Geoenvironmental Eng.*, vol. 127, no. 10, pp. 857–868, 2001.
[55] G.-C. Li, C.-C. Qi, Y.-T. Sun, X.-L. Tang, and B.-Q. Hou, "Experimental study on the softening characteristics of sandstone and mudstone in relation to moisture content," *Shock Vib.*, vol. 2017, pp. 1–14, Jan. 2017.

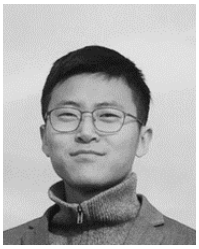

ZHUOQUN YU was born in Shandong, China, in 1995. He received the B.S. degree in mechanical engineering from the Qingdao University of Science and Technology, in 2017, where he is currently pursuing the Ph.D. degree in mechanical engineering. His research interests include mechanical engineering, mechanical properties of materials, and mining engineering.

YONGYAN WANG was born in Liaoning, China, in 1956. He received the Ph.D. degree in mining engineering from Liaoning Technology University. He is currently a Professor with the Qingdao University of Science and Technology. His research interests include rock mechanics and mechanical engineering.

HAO WANG received the M.Sc. degree in mechanical engineering from the Qingdao University of Science and Technology, in 2017. He is currently working as a Research Assistant with the Wuhan Institute of Rock and Soil Mechanics, Chinese Academy of Sciences. His research interests include rock mechanics experiments and microscopic structures of rock.